Protamine Functionalized Single-Walled Carbon Nanotubes for Stem Cell Labeling and In Vivo Raman/Magnetic Resonance/Photoacoustic Triple-Modal Imaging

Chao Wang, Xinxing Ma, Shuoqi Ye, Liang Cheng, Kai Yang, Liang Guo, Changhui Li, Yonggang Li, and Zhuang Liu**

Stem cells have shown great potential in regenerative medicine and attracted tremendous interests in recent years. Sensitive and reliable methods for stem cell labeling and in vivo tracking are thus urgently needed. Here, a novel approach to label human mesenchymal stem cells (hMSCs) with single-walled carbon nanotubes (SWNTs) for in vivo tracking by triple-modal imaging is presented. It is shown that polyethylene glycol (PEG) functionalized SWNTs conjugated with protamine (SWNT-PEG-PRO) exhibit extremely efficient cell entry into hMSCs, without affecting their proliferation and differentiation. The strong inherent resonance Raman scattering of SWNTs is used for in vitro and in vivo Raman imaging of SWNT-PEG-PRO-labeled hMSCs, enabling ultrasensitive in vivo detection of as few as 500 stem cells administrated into mice. On the other hand, the metallic catalyst nanoparticles attached on nanotubes can be utilized as the T2-contrast agent in magnetic resonance (MR) imaging of SWNT-labeled hMSCs. Moreover, in vivo photoacoustic imaging of hMSCs in mice is also demonstrated. The work reveals that SWNTs with appropriate surface functionalization have the potential to serve as multifunctional nanoprobes for stem cell labeling and multi-modal in vivo tracking.

1. Introduction

Mesenchymal stem cells (MSCs), also known as multipotent mesenchymal stromal cells, have presented promising applications in regenerative medicine, immunotherapy, and gene therapy in recent years.[1–3] Isolated from bone marrow, MSCs can be expanded in culture and differentiated into bone, cartilage, fat, muscle, and many other cell types.[4,5] MSCs are also able to migrate to and proliferate within sites of inflammation and tumors as part of the tissue remodeling process,[6–9] making them an attractive therapeutic tool for cellular therapy of various diseases including cancer.

The in vivo monitoring of stem cells after grafting is essential for better assessing and understanding their viability, migrational dynamics, differentiation processes, and regeneration potential.[10,11] Thus a reliable and cytocompatible labeling method for stem cells is critically needed. Transduction of MSCs with optical reporter genes such as green fluorescent protein (GFP) and luciferase is commonly used for stem cell tracking.[12–16] Reporter genes can be expressed only in live cells and will be passed on to progeny cells for cell tracking in a relatively long period of time. However, this method requires genetic modification of the stem cells and is primarily suitable for optical imaging, which may only be applied in small animal models, such as mice, with limited clinical value. Therefore, various efforts have also been devoted to the effective labeling and tracking of stem cells with other exogenous contrast agents, including fluorescent probes such as organic fluorophores or inorganic quantum dots (QDs),[17,18] radioactive isotopes,[13,19] and magnetic nanoparticles[20–23] for fluorescence, nuclear, and magnetic resonance (MR) imaging, respectively. Since each imaging modality has its own advantages and limits, multimodal imaging has become a new trend in molecular imaging as well as stem cell tracking.[24,25] Development of multifunctional imaging probes for efficient stem cell labeling

C. Wang, L. Cheng, K. Yang, Prof. Z. Liu
Jiangsu Key Laboratory for Carbon-Based Functional Materials & Devices
Institute of Functional Nano & Soft Materials Laboratory (FUNSOM)
Soochow University
Suzhou, Jiangsu 215123, China
E-mail: zliu@suda.edu.cn

DOI: 10.1002/adfm.201200133

X. X. Ma, Dr. L. Guo, Dr. Y. G. Li
Department of Radiology
the First Affiliated Hospital of Soochow University
Suzhou, Jiangsu, 215006, China
E-mail: liyonggang224@163.com
S. Q. Ye, Prof. C. H. Li
Department of Biomedical Engineering
College of Engineering
Peking University
Beijing, 100871, China

and in vivo multimodal tracking is therefore important to facilitate stem cell research.

Single-walled carbon nanotubes (SWNTs) such as 1D quantum wires show various unique physical and chemical properties that are useful in the area of nanomedicine, which include biological sensing, drug delivery, cancer therapy, and biomedical imaging.[26–38] Semiconducting SWNTs exhibit bandgap photoluminescence with emission in the near-infrared (NIR) to infrared-A (IR-A) region, which is an excellent optical window for imaging in biological systems.[32] We and others have also used the strong resonance-enhanced Raman scattering of SWNTs for in vitro and in vivo imaging.[30,39,40] The high chemical and photo stabilities of SWNTs allow long-term tracking and imaging in biological systems.[36] As one of the "darkest" materials in the world, SWNTs exhibit strong optical absorption from visible to NIR regions, making them promising contrast agents in photoacoustic tomography (PAT).[34,41] Furthermore, a number of groups have also utilized carbon nanotubes anchored with metallic nanoparticles, which are usually catalyst impurities formed during nanotube growth, as the T2 contrast agent in MR imaging.[40,44] On the other hand, although SWNTs without appropriate surface functionalization could induce certain toxicity to the treated cells or animals, a large number of reports have shown that SWNTs with biocomptiable coatings (e.g., polyethylene glycol (PEG) coating) appear to not be obviously toxic in vitro and in vivo in the tested dose ranges.[26,36,42,43] It has also been reported that functionalized SWNTs may be excreted from the injected animals by both renal and fecal excretion.[36,44,45] Therefore, SWNTs appear to be an excellent platform for multimodality biomedical imaging.

Here, we use SWNTs as novel multifunctional imaging probes for labeling and in vivo tracking of human MSCs (hMSCs). It is found that conjugation of protamine (PRO), an arginine-enriched protein, to PEG-functionalized SWNTs, is able to dramatically enhance the stem cell uptake of nanotubes by over an order of magnitude. No significant exocytosis of nanotubes is noticed after cell labeling with SWNT-PEG-PRO, potentially allowing long-term tracking of labeled cells. Careful studies on the proliferation and differentiation of SWNT-labeled hMSC reveal that the SWNT labeling renders no appreciable negative effect to the viability, regeneration, and proliferation of stem cells. Utilizing the resonance Raman signatures of SWNTs, as few as 500 stem cells administrated into mice are successfully detected, presenting a remarkable improvement in tracking sensitivity compared to a variety of previously reported stem cell

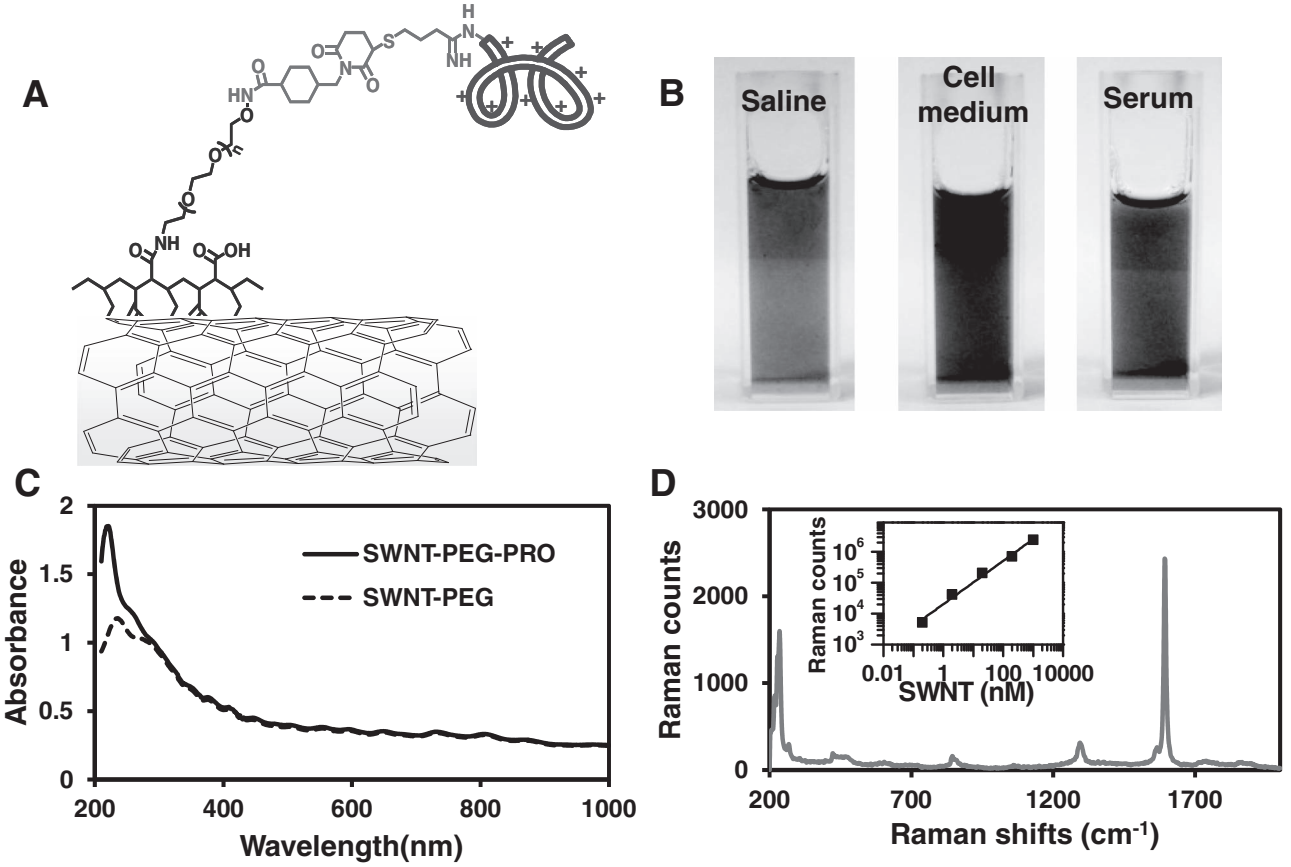

Figure 1. PEGylated SWNTs with protamine conjugation. A) A schematic drawing of SWNT-PEG-PRO. B) Photographs of SWNT-PEG-PRO in saline, cell medium, and serum under the ambient light, showing excellent stability of protamine conjugated nanotubes in various physiological solutions without any aggregation. C) UV-vis-NIR absorbance spectra of SWNT-PEG-PRO(blue) and SWNT-PEG(red). The absorption peak at ≈220 was due to protamine conjugated to SWNT. D) Raman spectrum of a SWNT-PEG-PRO solution excited at 785 nm. Inset: Raman intensity versus SWNT concentration. The G-band intensity of SWNTs was in linear relationship to the nanotube concentration.

tracking methods such as fluorescent imaging of QDs-labeled or GFP-expressing stem cells.[46,47] Triple-modal Raman/MR/PAT of SWNT-labeled hMSCs is demonstrated in mice.

2. Results and Discussion

2.1. Functionalization and Characterization of SWNT-PEG-PRO

SWNTs can be modified by either covalent or noncovalent functionalization to acquire water solubility for further biological use. However, covalent functionalization method often disrupts the nanotube structure and drastically weakens the photoluminescence and Raman scattering of SWNTs. Here, a non-covalent approach is employed to functionalize SWNTs with an amphiphilic polymer, amine-PEG-grafted poly(maleic anhydride-alt-1-octadecene) (C18PMH-PEG-NH2), by simple sonication of raw nanotubes in an aqueous solution of C18PMH-PEG-NH2. The obtained PEGylated SWNTs (SWNT-PEG) were centrifuged at a high *g*-force (21000 g) for 1 h to discard any unstable aggregates. Excess uncoated polymer was removed by vacuum filtration through a 100-nm filter membrane.

Protamine is an arginine-enriched protein with abundant positive charges known to enhance the cellular uptake of nanomaterials.[48] We conjugate SWNT-PEG with amine functional groups on PEG terminals to thiolated protamine via a bifunctional maleimide linker (**Figure 1**A).[31] Unconjugated protamine was thoroughly removed by centrifugal ultrafiltration. The synthesized SWNT-PEG-PRO conjugate exhibited excellent stability in various physiological solutions including saline, cell cultural medium, and serum (Figure 1B). The zeta-potential of SWNT-PEG-PRO was measured to be 4.7 mV, a large increase from that of SWNT-PEG at –23 mV.

The UV-visible-near infrared (UV-vis-NIR) absorbance spectrum of SWNT-PEG-PRO showed various small peaks which could be assigned to SWNTs with different chiralities. Compared to SWNT-PEG before protamine conjugation, SWNT-PEG-PRO exhibited a strong protamine absorption peak at ≈220 nm (Figure 1C). Raman spectrum of the SWNT-PEG-PRO solution excited at 785 nm showed the SWNT characteristic peaks at 200–300 cm^{-1}, ≈1400 cm^{-1}, and ≈1590 cm^{-1}, which were the radial breathing mode (RBM), D-band mode, and G-band mode, respectively. The Raman G-band peak of SWNTs, whose intensity was linearly related to the nanotube concentration (Figure 1D, inset), was utilized in our Raman imaging studies.

Carbon nanotubes anchored with metallic nanoparticles originated from the catalyst metals (e.g., Co, Fe, Ni, and Mo) have been utilized by several different groups as the T2-contrast agent in MR imaging.[49,50] As expected, a large number of metallic nanoparticles were observed in transmission electronic microscopy (TEM) images (**Figure 2**A) of the starting SWNT solid sample synthesized by the high-pressure CO disproportionation method (Hipco). Importantly, nanoparticles with diameter of 5–8 nm remained on the nanotubes even after PEG-functionalization and water-solubilization of SWNTs (Figure 2B). Energy-dispersive X-ray spectroscopy (EDS) of the SWNT-PEG sample revealed that the metallic nanoparticles anchored on nanotubes mainly contained Fe and likely also Co (Figure 2C), whose weight contents were measured by inductively coupled plasma atomic emission

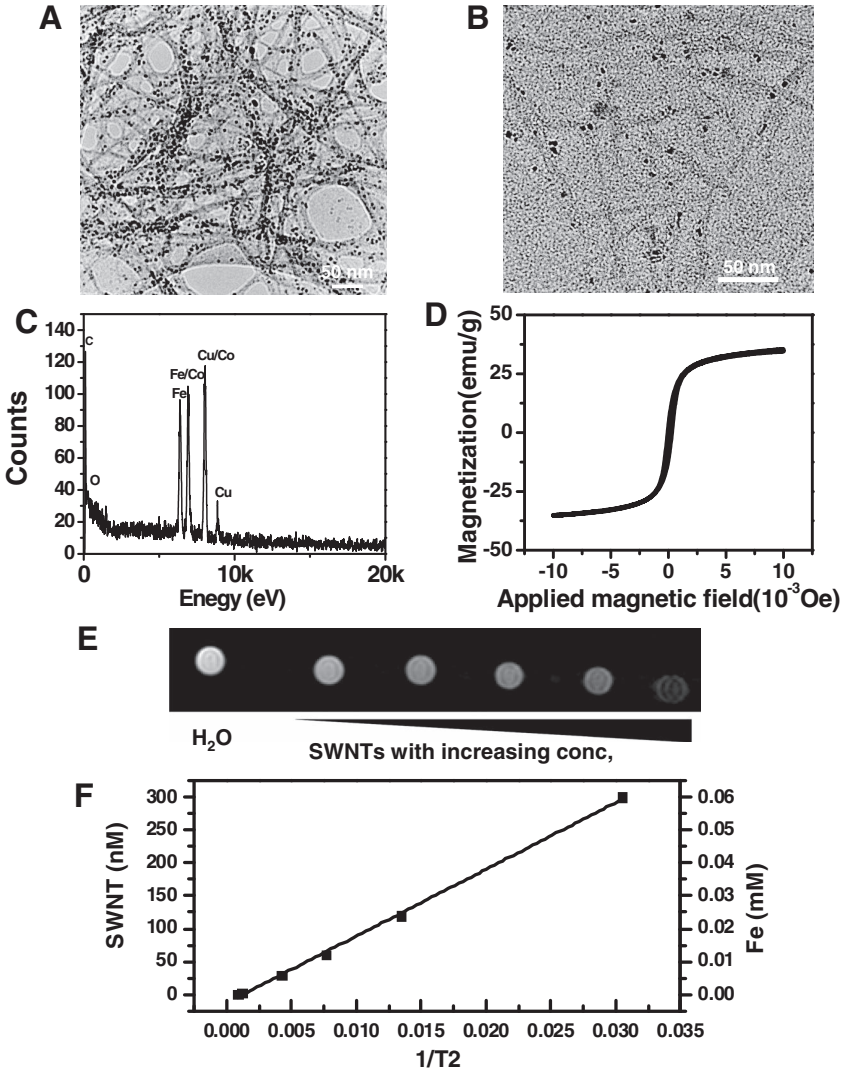

Figure 2. Magnetic properties of SWNTs. A,B) TEM images of raw Hipco SWNTs solid sample (A) and SWNT-PEG-PRO solution sample (B). A large number of metallic nanoparticles were observed on the surface of nanotubes. C) EDS of the SWNT-PEG-PRO sample showing strong Fe signals. D) The field-dependent magnetization loop of SWNT-PEG-PRO sample. The absence of hystersis loop suggested the superparamagnetic property of SWNTs. E) T2-weighted MR images of SWNT-PEG-PRO solutions at different concentrations. F) T2 relaxation rates (R2) of SWNT-PEG-PRO sample solutions at different SWNT and Fe concentrations.

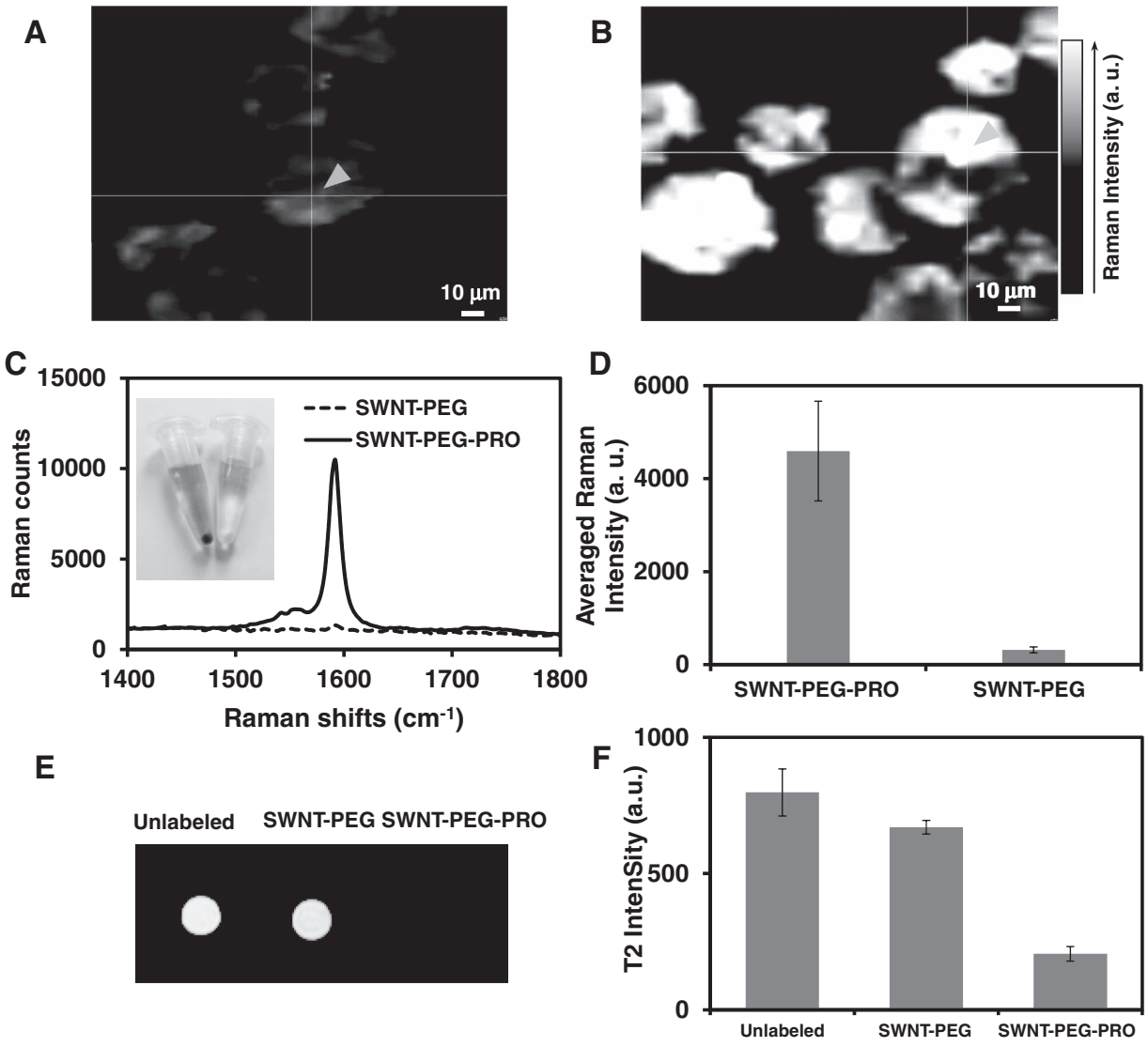

Figure 3. Stem cell labeling with SWNT-PEG and SWNT-PEG-PRO. A,B) Raman images of hMSCs incubated with SWNT-PEG (A) or SWNT-PEG-PRO (B) for 4 h. C) Raman spectra recorded from the pixels highlighted in (A) and (B). Inset: a photograph of hMSCs incubated with SWNT-PEG (right) or SWNT-PEG-PRO (left) after washing and centrifugation. D) Quantification of the mean Raman signal intensity per cell of hMSCs incubated with SWNT-PEG or SWNT-PEG-PRO. E) T2-weighted MR images of untreated, SWNT-PEG labeled and SWNT-PEG-PRO labeled hMSCs. Cells suspended in agarose gel were transferred into a 96-well plate for MR imaging. F) The T2-weighted MR signals of various hMSC samples indicated. Error bars are based on triplicated samples or measurements.

spectroscopy (ICP-AES) to be 6.26% (wt/wt) and 0.3% (wt/wt) for Fe and Co, respectively. Field-dependent magnetization measurements of the SWNT-PEG sample suggested the superparamagnetic nature of SWNTs attached with Fe/Co containing nanoparticles. An obvious concentration-dependent darkening effect was observed in T2-weighted MR images (Figure 2E), showing a rather high transverse relaxivity (r2) of 482.6 mM^{-1} s^{-1} on the basis of the Fe concentration (Figure 2F).

2.2. Stem Cell Labeling with SWNT-PEG-PRO

PEGylated SWNTs with and without protamine conjugation were then used for stem cell labeling. hMSCs collected from human bone marrow were incubated with 10 nM SWNT-PEG or SWNT-PEG-PRO for 4 h. After washing with phosphate buffered saline (PBS), cells were imaged using a HORIBA–Jobin–Yvon Raman microscope with a 785 nm laser as the excitation light source. It was found that hMSCs incubated with SWNT-PEG-PRO showed much stronger SWNT characteristic Raman scattering signals (G-band peak at ≈1590 cm^{-1}) compared to those incubated with SWNT-PEG (**Figure 3**A–C). The cells after SWNT-PEG-PRO labeling turned to dark gray whereas those treated with SWNT-PEG exhibited no obvious color change (Figure 3C, inset). To quantify the cell uptake of SWNTs, we followed a previously reported protocol[28] and integrated all spectra in a Raman spectroscopy image to get the total Raman intensity, which was divided by the number of cells in that image (Figure 3D). When hMSCs were incubated

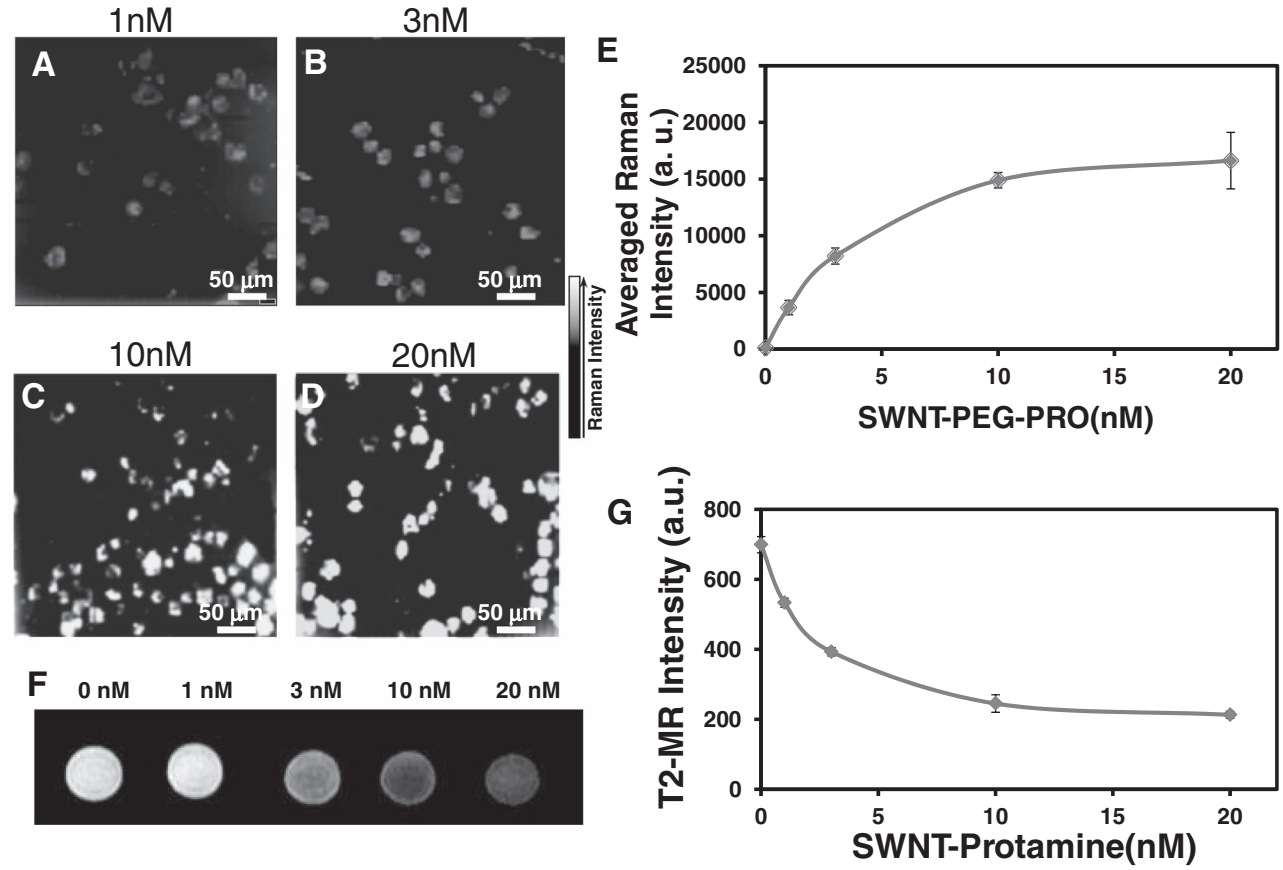

Figure 4. Concentration dependent hMCS labeling by SWNT-PEG-PRO. A–D) Raman images of hMSCs labeled with different concentrations of SWNT-PEG-PRO for 4 h. E) The averaged Raman intensity per cell quantified from Raman spectral images. F) T2-weighted MR image of hMSCs labeled with different concentrations of SWNT-PEG-PRO. G) Quantified T2 weighted MR signal intensity. Error bars are based on triplicated samples or measurements.

with SWNT-PEG-PRO, the mean Raman signal intensity on cells increased by ≈15 fold from that of cells exposed to SWNT-PEG. Control experiments uncovered that the SWNT-specific Raman signals on hMSCs incubated with a ultrahigh concentration of SWNT-PEG (100 nM) over a long period of time (12 h) was still much lower than that on cells incubated with SWNT-PEG-PRO at 10 nM for 4 h (Supporting Information Figure S1). Addition of free unconjugated protamine by itself offered no enhancement effect to the cellular uptake of SWNT-PEG (Supporting Information Figure S1), suggesting that it was the conjugation of protamine on PEGylated SWNTs that dramatically increased the cell uptake efficiency of nanotubes.

MR imaging was also used to evaluate the cell uptake efficiency of SWNT-PEG-PRO and SWNT-PEG. We observed that the T2-weighted MR signals of hMSCs decreased after either SWNT-PEG or SWNT-PEG-PRO treatment for 4 h at a nanotube concentration of 10 nM. As expected, the MR image of SWNT-PEG-PRO labeled cells appeared to be much darker compared to that of SWNT-PEG treated cells (Figure 3E,F).

To understand the cell uptake mechanism of SWNT-PEG-PRO, we labeled SWNT-PEG with a fluorescent dye, fluorescein, before protamine conjugation. Confocal fluorescence microscopy images revealed strong SWNT-fluorescence in the cell cytoplasm after hMSCs were incubated with fluorescein labeled SWNT-PEG-PRO for 4 h under 37 °C (Supporting Information Figure S2A). In marked contrast, dim fluorescence was observed only on the cell membrane but not in the cytoplasm if cell labeling was carried under 4 °C (Supporting Information Figure S2B). Further incubation of those cells under 37 °C, however, allowed cellular internalization of membrane-associated nanotubes (Supporting Information Figure S2C). These results suggested that the internalization of SWNT-PEG-PRO may possibly occur via the energy dependent endocytosis.[40,51]

To determine the optimal concentration of SWNT-PEG-PRO for stem cell labeling, hMSCs were incubated with SWNT-PEG-PRO for 4 h at varied nanotube concentrations of 1 nM, 3 nM, 10 nM, and 20 nM. Obvious increase in Raman signals and decrease in T2-weighted MR signals were observed as the increase of SWNT concentrations used during labeling (**Figure 4**). The signal intensities, however, started to saturate at concentrations above 10 nM. We thus chose 10 nM for the followed stem cell labeling studies.

A common problem in stem cell labeling and tracking is that the labeling probes could leak out from cells over time, leading to possible uptake of these probes by other nearby cells or macrophages and introducing false positive artifacts.[11,52] We thus studied this issue by a transwell culture system (**Figure 5**A–E). SWNT-PEG-PRO labeled hMSCs were cultured in the upper compartment of the transwell culture system, while unlabeled hMSCs were grown in the lower compartment. Control

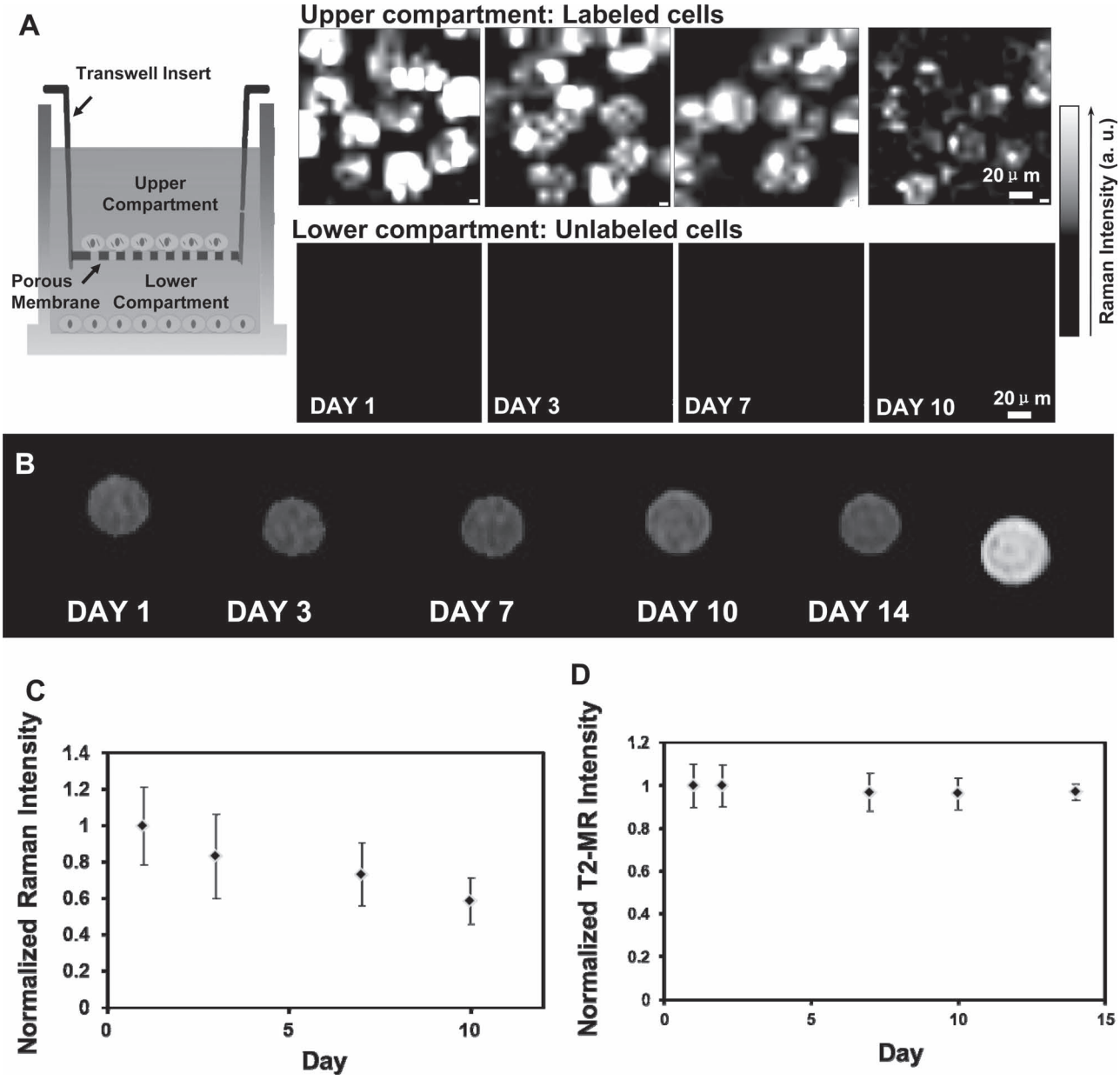

Figure 5. Long-term labeling of hMSCs. A) Raman images of SWNT-labeled hMSCs (the labeling SWNT concentration was 10 nM) at different time post labeling. Right inset is a schematic of the transwell system. The upper and lower rows of Raman images were SWNT-labeled and unlabeled cells cultured in the upper and lower compartments of the transwell plate, respectively. The micropores in the membrane with a diameter of 1000 nm allowed the diffusion of nanotubes across the membrane. No appreciable SWNT-characteristic Raman signals were detected from cells growing in the lower compartment. B) T2-weighted MR images of SWNT-labeled hMSCs at different time post labeling. C,D) Quantified Raman (C) and T2-weighted MR signals (D) from labeled hMSCs over time. While the averaged Raman intensity per cell showed an obvious trend of decrease due to cell proliferation, the MR signals were constant over 14 days since all cells in each sample were collected and fixed in the same volume of agarose gel for MR imaging. The starting cell confluence in each well was ≈40–50%. Error bars are based on triplicated samples or measurements.

experiment evidenced that nanotubes were able to freely diffuse through the microsporous membrane separating upper and lower compartments (Supporting Information Figure S3). Cells from both two compartments were imaged by the Raman microscope at different time points up to 10 days. Although it was found that the averaged Raman intensity per labeled cell was notably decreased likely owing to the dilution of intracellular nanotube-concentrations during cell proliferation (Figure 5G), no apparent Raman signal was observed in unlabeled hMSCs cultured in the lower compartment. We also collected all labeled cells for MR imaging and found that the T2-weighted MR contrasts of hMSCs were fairly stable for 2 weeks (Figure 5H). These data suggest

little, if any, exocytosis of SWNTs from labeled hMSCs, making it possible to use SWNT-PEG-PRO for long-term labeling of stem cells. Although a previous report has evidenced exocytosis of DNA-coated SWNTs from NIH-3T3 cells,[40] the intracellular fate of SWNTs may depend on cell types and surface coatings of nanotubes. Our data suggest very limited exocytosis of protamine conjugated PEGylated SWNTs from labeled hMSCs, promising the use of SWNT-PEG-PRO for long-term labeling of stem cells.

2.3. Interactions of SWNTs with Stem Cells

Numerous reports have explored the toxicology of carbon nanotubes in vitro and in vivo.[53–57] Although still under certain debate, it is generally accepted that the toxicity of carbon nanotubes is closely associated to their surface chemistry, and biocompatible surface coatings would significantly reduce the interference and toxicity of nanotubes in biological systems.[53–57] A number of groups have also studied the interactions between SWNTs and MSCs or other types of stem cells.[58–60] Barron et al.[58] reported COOH-functionalized SWNTs were not obviously toxic and showed little impact to the viability, proliferation, and differentiation of hMSCs. However, there are also reports suggesting that carbon nanotubes could inhibit the proliferation and differentiation of stem cells.[59] Careful examinations are thus required to understand how SWNT-PEG-PRO interacts with hMSCs before we further use those nanotubes for stem cell tracking.

Multiple approaches were used to evaluate the potential cellular toxicity of our SWNT-PEG-PRO to hMSCs from different aspects. Standard cell viability assay was first carried out to check the proliferation of SWNT-labeled hMSCs. HMSCs were incubated with varied concentrations of SWNT-PEG-PRO for 4 h and then transferred into fresh cell medium. The relative viabilities of hMSCs were assessed at different time points post SWNT-labeling (**Figure 6**A). No appreciable delay in cell proliferation was noted for hMSCs labeled with SWNT-PEG-PRO at nanotube concentrations up to 20 nM.

To further look for the potential cell damage caused by SWNTs, we also examined the release of lactate dehydrogenase (LDH) from SWNT-PEG-PRO-labeled hMSCs. LDH release is an indicator of cell membrane damage, which leads to cell necrosis. It was found that the levels of released LDH from SWNT-PEG-PRO treated hMSCs were normal compared to the untreated control, suggesting no obvious cell membrane damage induced by SWNT-labeling (Figure 6B).

Reactive oxygen species (ROS) are small molecules such as $\bullet O^{2-}$, •OH, and H_2O_2, which can damage biomacromolecules such as DNA, proteins, and lipids, resulting in a high degree of cytotoxicity. It has been found that a number of nanomaterials are able to induce oxidative stress to cells by generating ROS.[61,62] In our study, flow cytometric quantification of intracellular ROS by the dihydroethidine (DHE) probe revealed no significant increase in the percentage of DHE positive cells after treatment with different concentrations of SWNT-PEG-PRO (Figure 6C and Supporting Information Figure S4,S5), in marked contrast to the positive control cells treated with H_2O_2.

HMSCs can be differentiated into various cell types useful in tissue repairing and regeneration. We next investigated the impact of SWNT-PEG-PRO labeling to the differentiation

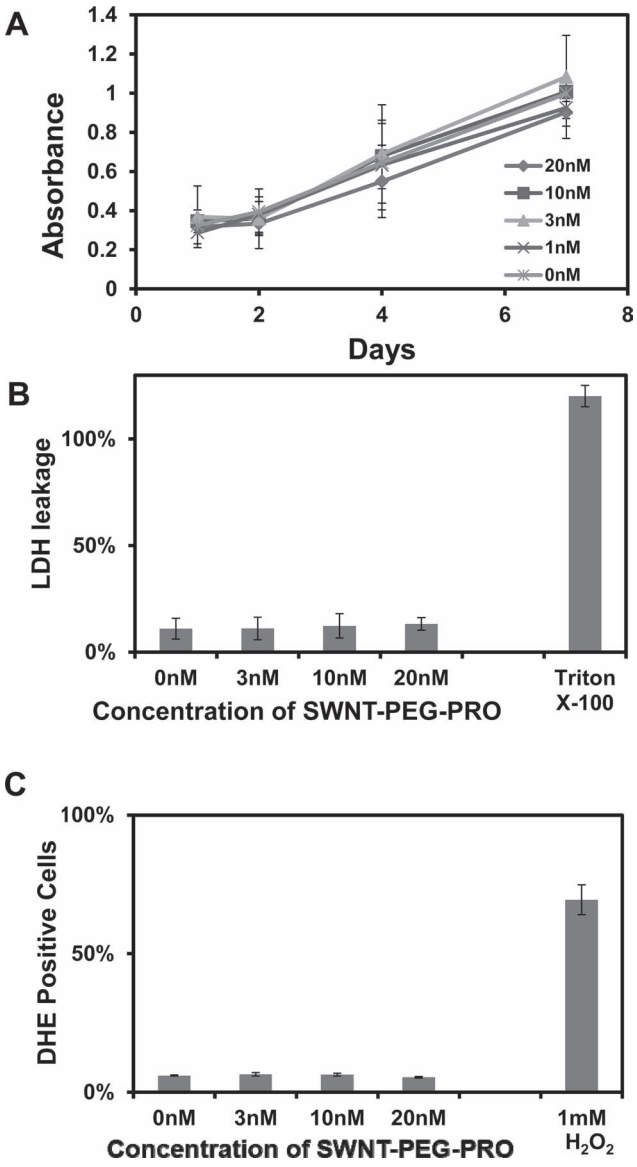

Figure 6. Toxicity of SWNT-PEG-PRO to hMSCs. A) Proliferation of hMSCs labeled with SWNT-PEG-PRO at various concentrations. The relative cell viabilities were evaluated by methyl thiazolyl tetrazolium (MTT) assay. The starting cell confluence in each well was ≈10% to allow the rapid cell proliferation. B) Percentage of LDH leakage of hMSCs after various treatments indicated. C) Generation of intracellular ROS determined by DHE staining and FACS measurement. Error bars are based on triplicate samples at minimum.

capability of hMSCs. To examine the pluripotency of hMSCs, SWNT-PEG-PRO labeled cells (10 nM of SWNTs) were cultured in adipogenic and osteogenic medium for 2 weeks. Following adipogenic differentiation, intracellular lipid droplets in SWNT-labeled hMSCs were observed in the same frequency as the control unlabeled hMSCs. Oil-red O (ORO) staining revealed the formation of lipid vacuoles by both unlabeled hMSCs as well as SWNT-labeled hMSCs (**Figure 7**D–F) during adipogenic differentiation. Colorimetric quantification of the extracted ORO from cells[63] at day 14 demonstrated the similar levels of adipogenic differentiation between unlabeled and SWNT-labeled hMSCs.

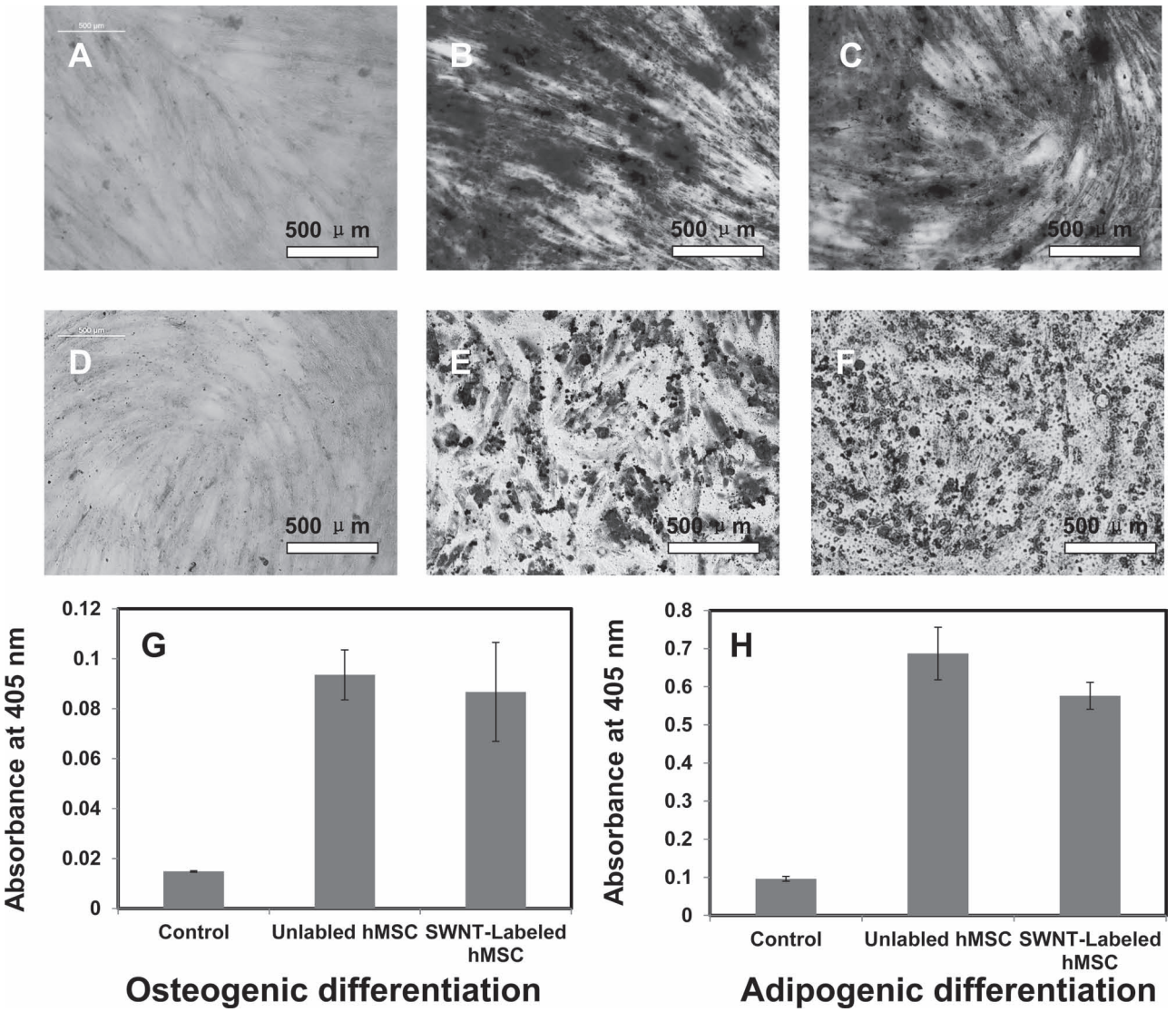

Figure 7. Differentiation of SWNT-labeled hMSCs. SWNT-PEG-PRO (10 nM) labeled cells were differentiated to osteoblasts and adipocytes in vitro and stained by ARS and ORO, respectively. A) ARS stained normally cultured hMSCs (non-differentiated). B,C) ARS stained unlabeled (B) and SWNT-labeled (C) hMSCs after being cultured in osteogenic culture for 14 days. D) ORO stained normally cultured hMSCs (non-differentiated). E,F) ORO stained unlabeled (E) and SWNT-labeled (F) hMSCs after being cultured in adipogenic culture for 14 days. G,H) Quantification of osteogenic differentiation (G) and adipogenic differentiation (H) of unlabeled and SWNT-labeled hMSCs after being cultured in the respective induction cultures for 14 days. The levels of differentiation were determined by measuring the 405 nm absorbance of ARS and ORO after they were extracted from cells. Error bars are based on triplicate samples.

Osteogenic differentiation of hMSC was also tested by culturing unlabeled and SWNT-labeled hMSCs in osteogenic medium for 14 days. Alizarin red S (ARS) was applied to stain calcium deposits, which were an indicator of osteogenic differentiation (Figure 7A–C). An ARS-based assay was also performed to quantify the level of osteogenesis by measuring the absorbance of ARS at 404 nm extracted from cells.[64] Both stained cell images and quantification data revealed that hMSCs labeled with SWNT-PEG-PRO had similar differentiate capability compared with normal unlabeled hMSCs.

Our date collectively suggest that SWNT-PEG-PRO has minimal toxicity to hMSCs at concentrations above the labeling concentration (10 nM), despite the ultraefficient cellular uptake of those protamine conjugated nanotubes. More importantly, the differentiation potential of hMSCs is also not noticeably affected by the SWNT-labeling. The SWNT-PEG-PRO developed here may indeed be a biocompatible probe applicable for stem cell labeling and tracking.

2.4. In Vivo Stem Cell Tracking by Triple-Modal Imaging

To explore the possibility and detection sensitivity of SWNT-based stem cell labeling and tracking, various numbers of hMSCs (2×10^4 to 500) labeled with SWNT-PEG-PRO at 10 nM were subcutaneously injected onto the back of a nude mouse.

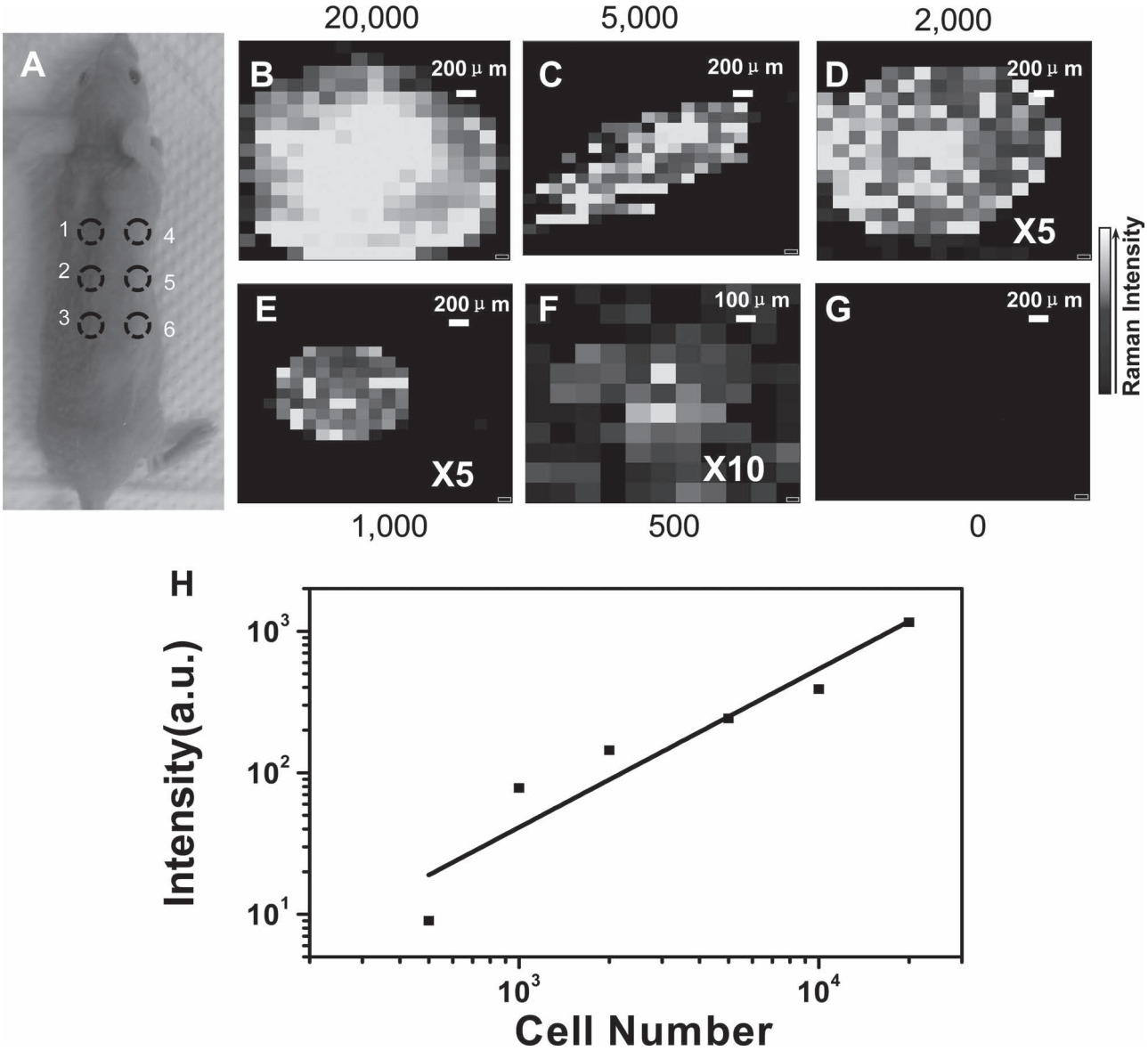

Figure 8. Detection sensitivity of SWNT-based stem cell labeling and Raman tracking. A) A photograph of a nude mouse used in the experiment. Different numbers of SWNT-labeled hMSCs (10 nM of SWNTs during labeling) were subcutaneously injected into the back of this mouse. B–G) Raman images of various numbers of hMSCs ($0–2 \times 10^4$) labeled with SWNT-PEG-PRO. H) Quantification of Raman signals showed nearly linear relationship between cell numbers and integrated total Raman intensities.

Raman mapping was carried out to image this live mouse under anaesthesia. A 785 nm laser was used as the excitation source for Raman spectroscopic mapping. Strong SWNT-characteristic G-band signals were detected on sites injected with hMSCs labeled by SWNT-PEG-PRO. Quantification of Raman signals showed nearly linear relationship between cell numbers and integrated Raman intensities. Even at the cell number as low as 500 (**Figure 8**), Raman signals from SWNTs were still clearly distinguishable from the background. The stem cell detection sensitivity of our SWNT-based labeling method is much higher than that of QD-labeled cells (detection limit ≈5000 cells)[47,65] under fluorescence imaging.[46,64] While the sensitivity of fluorescence imaging mainly suffers from the background autofluorescence of biological tissues, the rather sharp Raman emission peaks with full width at half-maximum (FWHM) of 1–2 nm can be easily differentiated from the autofluorescence background,[28] allowing greatly improved detection sensitivity.

Magnetic resonance imaging (MRI) is one of the most powerful non-invasive imaging techniques to image the whole human body for applications in clinical diagnosis and prognosis, providing both anatomic and functional information. On the other hand, PAT, a recently developed imaging technique, has also attracted significant interests in the field of biomedical imaging.[34,41,66–68] Compared with traditional optical imaging, PAT shows remarkably improved imaging depth due to the excellent soft tissue penetration ability of sound and is able to achieve

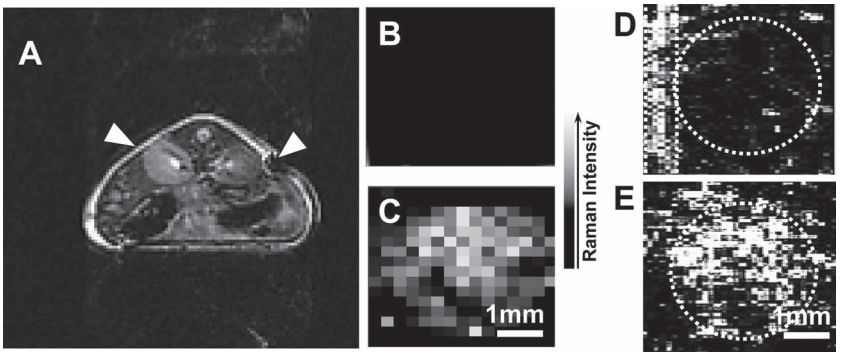

Figure 9. In vivo triple-modal imaging of SWNT-labeled hMSCs. Unlabeled and SWNT-labeled hMSCs (10 nM of SWNTs during labeling) were subcutaneously injected into the back of a nude mouse before imaging. A) In vivo T2-weighted MR image. Arrows pointed to the sites where unlabeled (left) and SWNT-labeled (right) hMSCs were injected. B,C) In vivo Raman images of unlabeled (B) and SWNT-labeled (C) hMSCs. D,E) In vivo PAT images of unlabeled (D) and SWNT-labeled (E) hMSCs. The circles highlighted the locations were hMSCs were injected. PA signals in the rectangle highlighted in D were from a blood vessel crossing this area.

cellular level resolution while imaging whole animals, which is advantageous for applications in stem cell tracking.[66,68] SWNTs with strong visible-to-NIR optical absorption and attached with magnetic metallic nanoparticles may thus be utilized as both PAT and MR imaging contrasts simultaneously.

In our experiment, hMSCs (2×10^5) labeled with or without SWNT-PEG-PRO were subcutaneously transplanted into the back of a nude mouse, which was then imaged under a 3-T clinical MRI scanner, a Raman spectroscopic microscope, and an in vivo PAT system (**Figure 9** and Supporting Information Figure S6). Compared to unlabeled cells, which were not detectable by the three different imaging modalities, strong Raman signals, obvious darkening effect in the T2-weighted MR image, and intense PA signals were observed from the site where the SWNT-labeled hMSCs were injected. It is worth noting that a 532 nm laser, which is not ideal for in vivo imaging, was used in the PAT experiments. Due to the light absorption by the blood hemoglobin, blood vasculatures surrounding the injection site caused certain interference to the SWNT PA signals from stem cells. This problem, however, could be easily resolved by using a NIR laser as the light source in our future studies.[34,41] The possible false MR or PAT contrast may also be easily excluded by Raman imaging of SWNT-specific signals, an obvious advantage for multimodal imaging that is able to circumvent limitations of a single imaging technique. Nevertheless, to our best knowledge, this is the first demonstration of using PAT for in vivo stem cell tracking.

At last, we conducted in vivo MR and Raman tracking of SWNT-labeled hMSCs over one week. hMSCs (2×10^6) labeled with SWNT-PEG-PRO were injected subcutaneously into the back of the nude mice. MR and Raman images were obtained 1, 3, and 7 days after transplantation (**Figure 10**). It was found that SWNT-labeled hMSCs could be clearly detected by both two imaging techniques for up to 7 days following subcutaneous transplantation. Our data evidence the capability of using our SWNT-labeling method for in vivo stem cell tracking over a relatively long period of time.

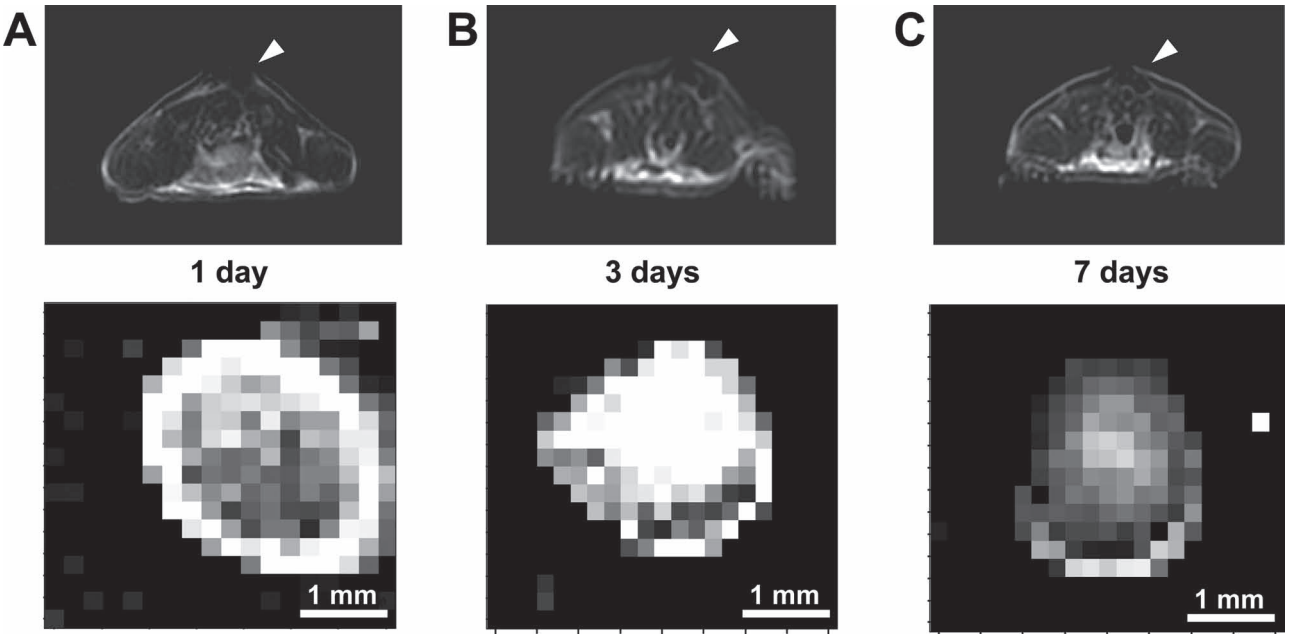

Figure 10. Long-term tracking hMSCs in vivo. hMSCs (2×10^6) labeled with SWNT-PEG-PRO were injected subcutaneously into the back of the nude mice. MR (the upper row) and Raman (the lower row) images were obtained 1 day (A), 3 days (B), and 7 days (C) after transplantation. Our imaging data suggested that hMSCs labeled with SWNT-PEG-PRO could be easily detected by both MR and Raman imaging techniques up to 7 days following subcutaneous transplantation.

3. Conclusion

We have used SWNTs as a novel multifunctional imaging probe for efficient stem cell labeling and multimodal in vivo tracking for the first time. It is found that the conjugation of protamine on PEGylated SWNTs could dramatically increase the uptake of nanotubes by hMSCs, allowing efficient cell labeling at a low SWNT concentration. Systematic in vitro tests uncover that our SWNT-PEG-PRO induces neither membrane damage nor oxidative stress to the labeled hMSCs. The proliferation and differentiation of hMSCs are also not notably affected by SWNT-labeling. Because of the high cell labeling efficiency and strong resonance Raman scattering of SWNTs, ultrasensitive in vivo detection of hMSCs with a detection limit down to 500 cells is realized by Raman imaging, which is a significant improvement from fluorescent imaging of GFP-expressing or QD-labeled stem cells.[46,47] In vivo Raman, MR, and PAT triple-modal imaging of SWNT-labeled hMSCs is further demonstrated in living mice. Moreover, the limited exocytosis of intracellular nanotubes allows tracking of SWNT-labeled hMSCs over a relative long period of time. Our results highlight the promise of well-functionalized SWNTs as novel biocompatible multimodal probes for stem cell labeling and tracking.

4. Experimental Section

Preparation of SWNT-PEG-PRO: C18PMH-PEG-NH2 polymer was synthesized according to previous reports.[69,70] Raw Hipco SWNTs at a concentration of 0.2 mg mL^{-1} were sonicated in a solution of C18PMH-PEG-NH2 polymer (3 mg mL^{-1}) for 1 h, yielding a black SWNT suspension, which was centrifuged at 21 000 g for 1 h to remove big aggregates. Excess polymer was removed by vacuum filtration of the nanotube solution through a 0.1 μm membrane. After repeated water washing, SWNTs collected on the filter membrane were re-suspended in water by a brief sonication and centrifuged at 21 000 g for 10 min to remove any aggregates formed during the filtration step. The obtained SWNT-PEG solution was stored at 4 °C for future use.

SWNT-PEG-PRO was synthesized by a two-step produce. First, 1 mL of SWNT-PEG (300 nM) was mixed with 1 mg of sulfosuccinimidyl-4-(*N*-maleimidomethyl)cyclohexane-1-carboxylate (Sulfo-SMCC, Pierce) in phosphate buffered saline (PBS, pH 7.4). After 2 h of reaction, excess Sulfo-SMCC was removed using a centrifugal filter device (molecular weight cut-off MWCO = 100 kDa) to purify the SMCC active SWNTs. In the meantime, protamine (Sigma, 10 mg mL^{-1}) was thiolated by reacting with the Traut's Reagent (2-iminothiolane, Pierce) in PBS (pH 7.4) at a molar ratio of 1:2 for 2 h at 4 °C. At last, the SMCC activated SWNT-PEG and protamine-SH was mixed in PBS (pH 7.4) at a molar ratio of SWNT: Protamine = 1:5000. After 24 h reaction at 4 °C, excess protamine was removed using the centrifugal filter device (MWCO = 100 kDa). The obtained SWNT-PEG-PRO was stored at 4 °C until use. The SWNT concentration was quantified by a molar extinction coefficient of 7.9×10^6 $M^{-1}cm^{-1}$ at 808 nm (assuming nanotubes have an average length of 150 nm and an averaged diameter of 1.2 nm).[29,71]

Cell Culture: hMSCs were a gift from the Shanghai Blood Center and were cultured in low-glucose Dulbecco's modified Eagle medium (L-DMEM, Hyclone) supplemented with 10% fetal bovine serum (FBS) (Gibco) and 1% penicillin/streptomycin (Gibco), with medium changed every 3–4 days. All cell cultures were maintained under the 5% CO_2 atmosphere at 37 °C.

Cell Labeling with SWNTs: SWNT-PEG or SWNT-PEG-PRO of various concentrations were incubated with hMSCs in six-well (50 000 cells per well) or 96-well (1×10^3 cells per well) culture plates for 4 h, followed by repetitive washing with PBS to remove unbound SWNTs. Labeled cells were then cultured in fresh cell medium for desired periods of time. The cell proliferation was studied by measuring the cell viabilities using the standard MTT (Sigma-Aldrich) assay.

A transwell system was used to study whether SWNTs in labeled hMSCs were released and entered unlabeled hMSCs. hMSCs were cultured in the transwell insert (upper compartment) incorporating polyethylene terephthalate (PET) track-etched membranes (pore size of 1000 nm, BD Biosciences). Unlabeled hMSCs were cultured in the underlying plate well (lower compartment). At different time points, cells were digested with trypsin for Raman imaging.

ROS Assay: ROS production was evaluated by a hydroethidine (HE) probe known be oxidized by various oxidative agents. In brief, cells were treated for 24 h with different concentrations of SWNT-PEG-PRO. After trypsination, cells were centrifuged at 1000 rpm for 5 min, re-suspended in cell culture medium containing 1 μM HE (sigma), and analyzed using a flow cytometry (FACS Calibur from Becton-Dickinson).

LDH Assay: The cell membrane integrity can be determined by lactate dehydrogenase (LDH) leakage assay. LDH leakage was measured using a cytotoxicity detection kit (Promega Cat. 7891) following the vendor's protocol. In this experiment, hMSCs lysed by 1% Triton-X-100 were used as the positive control, while the cell-free medium was used as the negative control. The analysis was performed with a microplate reader (Bio-Rad).

Differentiation of Loaded MSC: Differentiation capacity of hMSCs was assessed by adipogenic and osteogenic differentiation-induction experiments. For adipogenic differentiation, hMSCs with or without SWNT-labeling were plated at a density of 2×10^4 cells cm^{-2} in a 24-well culture plate. When the cells were confluent, adipogenic differentiation was initiated by adding an induction culture containing L-DMEM cell medium supplemented with 10% FBS, 1 μM dexamethasone, 60 μM indomethacin, 5 μg mL^{-1} insulin, and 0.5 mM 3-isobutyl-l-methylxanthine. The induction medium was changed every 3 days until the 14th day. Cells were then fixed and stained with 0.3% Oil-red-O.

The osteogenic induction culture was L-DMEM supplemented with 10% FBS, 0.1 μM dexamethasone, 50 mg L^{-1} ascorbic acid, and 10 mM *β*-glycerophosphate. The culture medium was replaced every 3–4 days. After being cultured for 14 days, cells were fixed and stained by Alizarin red S.

In Vitro Raman Imaging of SWNT-Labeled hMSCs: Raman spectroscopic imaging was performed using a LabRam HR Raman microscope (Horiba Jobin Yvon Inc.) with a 785 nm laser as the excitation source and a 50× objective for Raman mapping. A drop of cell suspension was sealed between two thin quartz cover-slides for imaging. Step distances of 2–10 μm were used during mapping, depending on the image sizes. The spectral integration time was 0.1 s at each mapping point. A low laser power of 8 mW (10% of initially total power of the laser) was used during imaging to avoid heating of SWNT-labeled cells.

In Vivo Raman, MR, and PAT Triple-Modal Imaging of SWNT-Labeled hMSCs: Athymic nudemice (weight ≈ 20 g) were purchased from Suzhou Belda Bio-Pharmaceutical Co. and used under protocols approved by Soochow University Laboratory Animal Center.

Raman images were obtained by using a Raman point mapping method. A computer-controlled *x*–*y* translation stage was used to rasterscan the mouse, creating a spectral image by measuring the Raman spectrum of each individual pixel in the area of interest. A 785 nm laser (80 mW) and a 10× objective were used during imaging.

MR imaging was accomplished with a 3-T clinical MRI scanner equipped with a special coil used for small animal imaging.

PAT imaging was carried out on a home-made acoustic-resolution photoacoustic microscopy (AR-PAM) system (Supporting Information Figure S6), similar to the previous reported system.[66] During imaging, laser pulses (532 nm from a Nd:YAG laser with a repetition rate of 10 Hz and a pulse width of 10 ns) were coupled into a fiber, went through a dark-field illumination path, and finally reached the tissue under skin. A focused ultrasonic transducer (numerical aperture: 0.4, center frequency at 20 MHz) was used to detect PA signals. Mounting on an *x*–*y* motorized translational stage, the PAM system performed a 2D raster scanning with a step distance of 100 μm.

Acknowledgements

This work was partially supported by National Basic Research Program (973 Program) of China (2012CB932600, 2011CB911002), the National Natural Science Foundation of China (51132006, 51002100, 81171394), the Natural Science Fund of Jiangsu Province (09KJB320016, SBK201122654), and A Project Funded by the Priority Academic Program Development of Jiangsu Higher Education Institutions.

Received: January 15, 2012
Revised: February 9, 2012
Published online: March 13, 2012

[1] P. Bianco, P. G. Robey, P. J. Simmons, *Cell Stem Cell* **2008**, *2*, 313.
[2] L. S. Sasportas, R. Kasmieh, H. Wakimoto, S. Hingtgen, J. A. J. M. van de Water, G. Mohapatra, J. L. Figueiredo, R. L. Martuza, R. Weissleder, K. Shah, *Proc. Natl. Acad. Sci. USA* **2009**, *106*, 4822.
[3] G. Chamberlain, J. Fox, B. Ashton, J. Middleton, *Stem Cells* **2007**, *25*, 2739.
[4] M. F. Pittenger, A. M. Mackay, S. C. Beck, R. K. Jaiswal, R. Douglas, J. D. Mosca, M. A. Moorman, D. W. Simonetti, S. Craig, D. R. Marshak, *Science* **1999**, *284*, 143.
[5] D. J. Prockop, *Science* **2001**, *293*, 211.
[6] A. Nakamizo, F. Marini, T. Amano, A. Khan, M. Studeny, J. Gumin, J. Chen, S. Hentschel, G. Vecil, J. Dembinski, M. Andreeff, F. F. Lang, *Cancer Res.* **2005**, *65*, 3307.
[7] M. Sasaki, R. Abe, Y. Fujita, S. Ando, D. Inokuma, H. Shimizu, *Immunol. J.* **2008**, *180*, 2581.
[8] K. Satake, J. Lou, L. G. Lenke, *Spine* **2004**, *29*, 1971.
[9] B. Neuhuber, B. T. Himes, J. S. Shumsky, G. Gallo, I. Fischer, *Brain Res.* **2005**, *1035*, 73.
[10] J. M. Karp, G. S. L. Teol, *Cell Stem Cell* **2009**, *4*, 206.
[11] J. V. Frangioni, R. J. Hajjar, *Circulation* **2004**, *110*, 3378.
[12] H. Kawada, J. Fujita, K. Kinjo, Y. Matsuzaki, M. Tsuma, H. Miyatake, Y. Muguruma, H. Okano, T. Hotta, K. Fukuda, K. Ando, *Blood* **2004**, *104*, 736a.
[13] I. M. Barbash, P. Chouraqui, J. Baron, M. S. Feinberg, S. Etzion, A. Tessone, L. Miller, E. Guetta, D. Zipori, L. H. Kedes, R. A. Kloner, J. Leor, *Circulation* **2003**, *108*, 863.
[14] H. Wang, F. Cao, A. De, Y. Cao, C. Contag, S. S. Gambhir, J. C. Wu, X. Chen, *Stem Cells* **2009**, *27*, 1548.
[15] S. Kidd, E. Spaeth, J. L. Dembinski, M. Dietrich, K. Watson, A. Klopp, V. L. Battula, M. Weil, M. Andreeff, F. C. Marini, *Stem Cells* **2009**, *27*, 2614.
[16] T. E. Meyerrose, D. A. De Ugarte, A. A. Hofling, P. E. Herrbrich, T. D. Cordonnier, L. D. Shultz, J. C. Eagon, L. Wirthlin, M. S. Sands, M. A. Hedrick, J. A. Nolta, *Stem Cells* **2007**, *25*, 220.
[17] L. S. Shah, P. A. Clark, E. K. Moioli, M. A. Stroscio, J. J. Mao, *Nano Lett.* **2007**, *7*, 3071.
[18] A. B. Rosen, D. J. Kelly, A. J. Schuldt, J. Lu, I. A. Potapova, S. V. Doronin, K. J. Robichaud, R. B. Robinson, M. R. Rosen, P. R. Brink, G. R. Gaudette, I. S. Cohen, *Stem Cells* **2007**, *25*, 2128.
[19] T. Freyman, G. Polin, H. Osman, J. Crary, M. Lu, L. Cheng, M. Palasis, R. L. Wilensky, *Eur. Heart J.* **2006**, *27*, 1114.
[20] H. J. Chung, H. Lee, K. H. Bae, Y. Lee, J. Park, S. W. Cho, J. Y. Hwang, H. Park, R. Langer, D. Anderson, T. G. Park, *ACS Nano* **2011**, *5*, 4329.
[21] J. K. Hsiao, M. F. Tai, H. H. Chu, S. T. Chen, H. Li, D. M. Lai, S. T. Hsieh, J. L. Wang, H. M. Liu, *Magn. Reson. Med.* **2007**, *58*, 717.
[22] Y. S. Song, J. H. Ku, *Neurourol. Urodyn.* **2007**, *26*, 584.
[23] L. Y. Chien, J. K. Hsiao, S. C. Hsu, M. Yao, C. W. Lu, H. M. Liu, Y. C. Chen, C. S. Yang, D. M. Huang, *Biomaterials* **2011**, *32*, 3275.
[24] J. M. Hill, A. J. Dick, V. K. Raman, R. B. Thompson, Z. X. Yu, K. A. Hinds, B. S. S. Pessanha, M. A. Guttman, T. R. Varney, B. J. Martin, C. E. Dunbar, E. R. McVeigh, R. J. Lederman, *Circulation* **2003**, *108*, 1009.
[25] S. A. Wickline, G. M. Lanza, *Circulation* **2003**, *107*, 1092.
[26] Z. Liu, S. Tabakman, K. Welsher, H. J. Dai, *Nano Res.* **2009**, *2*, 85.
[27] Z. A. Liu, K. Yang, S. T. Lee, *J. Mater. Chem.* **2011**, *21*, 586.
[28] Z. Liu, S. Tabakman, S. Sherlock, X. Li, Z. Chen, K. Jiang, S. Fan, H. Dai, *Nano Res.* **2010**, *3*, 222.
[29] K. Welsher, Z. Liu, S. P. Sherlock, J. T. Robinson, Z. Chen, D. Daranciang, H. J. Dai, *Nat. Nanotechnol.* **2009**, *4*, 773.
[30] Z. A. Liu, X. L. Li, S. M. Tabakman, K. L. Jiang, S. S. Fan, H. J. Dai, *J. Am. Chem. Soc.* **2008**, *130*, 13540.
[31] Z. Liu, S. M. Tabakman, Z. Chen, H. J. Dai, *Nat. Protocols* **2009**, *4*, 1372.
[32] K. Welsher, Z. Liu, D. Daranciang, H. Dai, *Nano Lett.* **2008**, *8*, 586.
[33] Z. Chen, S. M. Tabakman, A. P. Goodwin, M. G. Kattah, D. Daranciang, X. R. Wang, G. Y. Zhang, X. L. Li, Z. Liu, P. J. Utz, K. L. Jiang, S. S. Fan, H. J. Dai, *Nat. Biotechnol.* **2008**, *26*, 1285.
[34] A. de la Zerda, Z. A. Liu, S. Bodapati, R. Teed, S. Vaithilingam, B. T. Khuri-Yakub, X. Y. Chen, S. S. Gambhir, H. J. Dai, *Nano Lett.* **2010**, *10*, 2168.
[35] S. Dhar, Z. Liu, J. Thomale, S. J. Lippard, H. J. Dai, *J. Am. Chem. Soc.* **2008**, *130*, 11467.
[36] Z. Liu, C. Davis, W. B. Cai, L. He, X. Y. Chen, H. J. Dai, *Proc. Natl. Acad. Sci. USA* **2008**, *105*, 1410.
[37] Z. Liu, K. Chen, C. Davis, S. Sherlock, Q. Z. Cao, X. Y. Chen, H. J. Dai, *Cancer Res.* **2008**, *68*, 6652.
[38] F. Zhou, D. Xing, B. Wu, S. Wu, Z. Ou, W. R. Chen, *Nano Lett.* **2010**, *10*, 1677.
[39] C. Zavaleta, A. de la Zerda, Z. Liu, S. Keren, Z. Cheng, M. Schipper, X. Chen, H. Dai, S. S. Gambhir, *Nano Lett.* **2008**, *8*, 2800.
[40] H. Jin, D. A. Heller, M. S. Strano, *Nano Lett.* **2008**, *8*, 1577.
[41] A. DeLa Zerda, C. Zavaleta, S. Keren, S. Vaithilingam, S. Bodapati, Z. Liu, J. Levi, B. R. Smith, T. J. Ma, O. Oralkan, Z. Cheng, X. Y. Chen, H. J. Dai, B. T. Khuri-Yakub, S. S. Gambhir, *Nat. Nanotechnol.* **2008**, *3*, 557.
[42] M. L. Schipper, N. Nakayama-Ratchford, C. R. Davis, N. W. Kam, P. Chu, Z. Liu, X. Sun, H. Dai, S. S. Gambhir, *Nat. Nanotechnol.* **2008**, *3*, 216.
[43] Z. Liu, W. Cai, L. He, N. Nakayama, K. Chen, X. Sun, X. Chen, H. Dai, *Nat. Nanotechnol.* **2007**, *2*, 47.
[44] K. Kostarelos, A. Bianco, M. Prato, *Nat. Nanotechnol.* **2009**, *4*, 627.
[45] D. Georgin, B. Czarny, M. Botquin, M. Mayne-L'Hermite, M. Pinault, B. Bouchet-Fabre, M. Carriere, J. L. Poncy, Q. Chau, R. Maximilien, V. Dive, F. Taran, *J. Am. Chem. Soc.* **2009**, *131*, 14658.
[46] F. Belema-Bedada, S. Uchida, A. Martire, S. Kostin, T. Braun, *Cell Stem Cell* **2008**, *2*, 566.
[47] H. Yukawa, Y. Kagami, M. Watanabe, K. Oishi, Y. Miyamoto, Y. Okamoto, M. Tokeshi, N. Kaji, H. Noguchi, K. Ono, M. Sawada, Y. Baba, N. Hamajima, S. Hayashi, *Biomaterials* **2010**, *31*, 4094.
[48] A. S. Arbab, G. T. Yocum, H. Kalish, E. K. Jordan, S. A. Anderson, A. Y. Khakoo, E. J. Read, J. A. Frank, *Blood* **2004**, *104*, 1217.
[49] J. H. Choi, F. T. Nguyen, P. W. Barone, D. A. Heller, A. E. Moll, D. Patel, S. A. Boppart, M. S. Strano, *Nano Lett.* **2007**, *7*, 861.
[50] A. Al Faraj, K. Cieslar, G. Lacroix, S. Gaillard, E. Canot-Soulas, Y. Cremillieux, *Nano Lett.* **2009**, *9*, 1023.
[51] Z. Liu, M. Winters, M. Holodniy, H. J. Dai, *Angew. Chem. Int. Ed.* **2007**, *46*, 2023.
[52] K. Hoshino, H. Q. Ly, J. V. Frangioni, R. J. Hajjar, *Prog. Cardiovasc. Dis.* **2007**, *49*, 414.
[53] Y. Zhang, Y. Xu, Z. Li, T. Chen, S. M. Lantz, P. C. Howard, M. G. Paule, W. Slikker, F. Watanabe, T. Mustafa, A. S. Biris, S. F. Ali, *ACS Nano* **2011**, *5*, 7020.
[54] M. L. Schipper, N. Nakayama-Ratchford, C. R. Davis, N. W. S. Kam, P. Chu, Z. Liu, X. M. Sun, H. J. Dai, S. S. Gambhir, *Nat. Nanotechnol.* **2008**, *3*, 216.

[55] H. Dumortier, S. Lacotte, G. Pastorin, R. Marega, W. Wu, D. Bonifazi, J. P. Briand, M. Prato, S. Muller, A. Bianco, *Nano Lett.* **2006**, *6*, 1522.
[56] A. E. Porter, M. Gass, J. S. Bendall, K. Muller, A. Goode, J. N. Skepper, P. A. Midgley, M. Welland, *ACS Nano* **2009**, *3*, 1485.
[57] P. Wu, X. Chen, N. Hu, U. C. Tam, O. Blixt, A. Zettl, C. R. Bertozzi, *Angew. Chem. Int. Ed.* **2008**, *47*, 5022.
[58] E. Mooney, P. Dockery, U. Greiser, M. Murphy, V. Barron, *Nano Lett.* **2008**, *8*, 2137.
[59] D. Liu, C. Yi, D. Zhang, J. Zhang, M. Yang, *ACS Nano* **2010**, *4*, 2185.
[60] H. Gul, W. Lu, P. Xu, J. Xing, J. Chen, *Nanotechnology* **2010**, *21*, 155101.
[61] A. Nel, T. Xia, L. Madler, N. Li, *Science* **2006**, *311*, 622.
[62] L. X. Shi, B. Hernandez, M. Selke, *J. Am. Chem. Soc.* **2006**, *128*, 6278.
[63] C. A. Gregory, A. S. Perry, E. Reyes, A. Conley, W. G. Gunn, D. J. Prockop, *J. Biol. Chem.* **2005**, *280*, 2309.
[64] C. A. Gregory, W. G. Gunn, A. Peister, D. J. Prockop, *Anal. Biochem.* **2004**, *329*, 77.
[65] D. L. Kraitchman, M. Tatsumi, W. D. Gilson, T. Ishimori, D. Kedziorek, P. Walczak, P. Segars, H. H. Chen, D. Fritzges, I. Izbudak, R. G. Young, M. Marcelino, M. F. Pittenger, M. Solaiyappan, R. C. Boston, B. M. W. Tsui, R. L. Wahl, J. W. M. Bulte, *Circulation* **2005**, *112*, 1451.
[66] K. Maslov, G. Stoica, L. H. V. Wang, *Opt. Lett.* **2005**, *30*, 625.
[67] K. H. Song, C. H. Kim, C. M. Cobley, Y. N. Xia, L. V. Wang, *Nano Lett.* **2009**, *9*, 183.
[68] V. Ntziachristos, J. Ripoll, L. H. V. Wang, R. Weissleder, *Nat. Biotechnol.* **2005**, *23*, 313.
[69] C. Wang, L. Cheng, Z. Liu, *Biomaterials* **2011**, *32*, 1110.
[70] X. W. Liu, H. Q. Tao, K. Yang, S. A. Zhang, S. T. Lee, Z. A. Liu, *Biomaterials* **2011**, *32*, 144.
[71] N. W. S. Kam, M. O'Connell, J. A. Wisdom, H. J. Dai, *Proc. Natl. Acad. Sci. USA* **2005**, *102*, 11600.